# Added-mass estimation in the structural response of tidal turbine blades

E. Mascrier, Grégory Pinon, F. Zilic de Arcos

# Added-mass estimation in the structural response of tidal turbine blades

E. Mascrier & G. Pinon
*Laboratoire Ondes et Milieux Complexes - Normandie Univ, UNIHAVRE, CNRS, Le Havre, France*

F. Zilic de Arcos
*Department of Engineering Science, University of Oxford, Oxford, United Kingdom*

ABSTRACT:
Aero- and hydrodynamic forces induce deformations on rotor blades and rigid-body motions in the case of floating systems. The acceleration of a volume of fluid perturbed by a moving body and commonly referred to as added-mass, affects the loads and structural response. Previous research describe the added-mass with simplified formulation. Such models are generally based on two assumptions: that the volume of fluid influenced by the blade section is equivalent to that of a cylinder with a radius similar to the local blade chord, and that the added-mass coefficient for a foil is equal to the unit. This study re-examines the concept of added-mass and the assumptions used in engineering models by simulate oscillating two-dimensional foil sections at different motion amplitudes, frequencies, and inflow speeds. The data derived from the foil CFD simulations highlight discrepancies between simplified models and a dependency of added-mass coefficients on motion frequency and amplitude.

## 1 INTRODUCTION

Tidal turbines are likely to be affected by substantial load fluctuations during operation. Waves, turbulence or the tidal cycle are some of the flow phenomena occurring at different temporal and spatial scales that affect rotor loads. The varying forces result in blade deformations, which affect hydrodynamic loads as well. The fluid-structure interactions between tidal rotor blades and the surrounding flow are tightly coupled and dynamic. It is, thus, the dynamic response of the coupled system that could affect the long term reliability of tidal stream energy converters (Satrio et al., 2024).

Tidal turbine blades can move and rotate as a consequence not only of the rotor spinning, but also due to, e.g., deformations (Zilic de Arcos et al., 2022) or the motions of a floating support platform (Zhang et al., 2015). As a turbine moves, a portion of the fluid surrounding the blades is displaced. The added-mass effects are a consequence of the fluid surrounding the rotor being accelerated, while the high density of water compared to air suggests that effects can be significant. These effects include changes to the dynamic structural response of the blades due to increased inertial loads.

Added-mass is a topic that has been explored in different areas such as ships (Ghassemi & Yari, 2011; Lou & Cui, 2021; Parsons et al., 1980), or underwater vehicles (Javanmard et al., 2020; Moelyadi & Riswandi, 2018). In these articles, studies were performed through experiments (Sedlar et al., 2011) or numerical simulations. While numerical models are versatile, there are challenges due to the complexity of the problem.

While relatively unexplored, the added-mass impact on tidal stream energy is likely to be relevant. In this article, the scope is on revisiting added-mass effects on two-dimensional sections of a tidal rotor blade. The ultimate goal is to support the development of improved engineering models capable of producing more accurate load predictions through an increased physical understanding of the added-mass phenomena.

Directly modeling the added-mass in fluid-structure interaction remains complex. Lefrançois, 2017 describes a method to compute the added-mass matrix based on the velocity potential. This method requires resolving and sampling the flow at each time step, a computationally expensive approach.

Simplified models to account for added-mass effects in the context of blade-element models have also been proposed. Maniaci & Li, 2012 proposed a model to describe the inertial loads on a tidal turbine blade based on the analytical definition of added-mass on a flat plate. Similar approaches were also adopted by

Faudot & Dahlhaug, 2012, Murray et al., 2018, Guo et al., 2018, Zilic de Arcos et al., 2023. The validity of the assumptions and generality of the coefficients used in the engineering modeling of added mass effects on tidal turbine blades remains, to the best of our knowledge, untested.

In this paper, we investigate the effect of added-mass through Reynolds-Averaged Navier Stokes (RANS) CFD simulations with OpenFOAM. The study is performed on a cylinder and a RISØ-A1-24 aerofoil (Schluntz & Willden, 2015). The numerical setup is validated with experimental data, presented in Section 3.1, comparing the steady-state lift and drag coefficients on the aerofoil. Different angles of attack $\alpha$ under steady inflow conditions are considered. The validation is followed in Section 3.2 by transient simulations where harmonic vertical motions of varying frequency and amplitude are prescribed on a cylinder and an airfoil. Results are compared with the engineering models for added-mass presented in Section 2.2.

## 2 METHODS

### 2.1 *Generalised Added-Mass Theory*

A tidal turbine blade moving in water affects a volume of fluid surrounding the structure. This mass of fluid is considered as a virtual mass added to the blade and, thus, referred to as added-mass. The added-mass effects are observed as an inertial force opposite to the structure motion (Brennen, 1982). The added-mass force is defined as :

$$F_{AM} = -M_{ij}A_j \tag{1}$$

with $M_{ij}$ the added-mass matrix and $A_j$ the structure acceleration. $M_{ij}$ is a 6x6 matrix containing 3 translation directions and 3 rotation angles. For the structure acceleration, $j = 1, 2, 3$ corresponds to the 3 Cartesian acceleration and $j = 4, 5, 6$ corresponds to the 3 angular accelerations.

The elements composing the added-mass matrix from Eq. (1) can be expressed by a velocity potential $\phi$ :

$$M_{ij} = \rho \int_A \phi_i \frac{\partial \phi_j}{\partial n} dA \;\; with \;\; \phi = \nabla U \tag{2}$$

with $\rho$ the fluid density, $\phi_i$ the velocity potential resulting from a unit velocity of the structure in the $i$ direction, $A$ the surface area and $n$ the normal to the surface. Analytic solutions can be found for simple geometries like cylinders or plates in 2D or 3D. For example, the added-mass of a 2D plate in motion normal to its face is (Brennen, 1982):

$$m_{Plate} = \rho\pi\frac{a^2}{4} \tag{3}$$

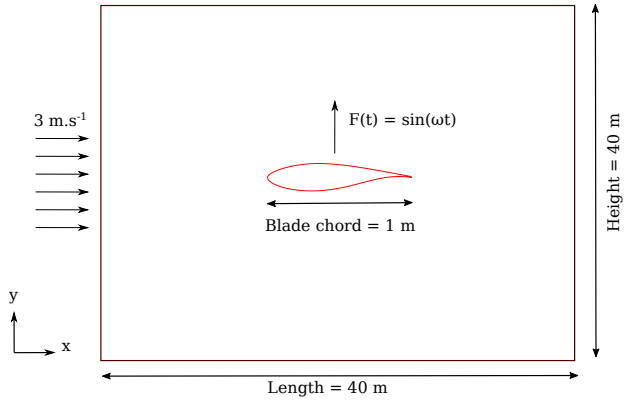


Figure 1: Numerical configuration for the RISØ-A1-24

with $a$ the plate length. Eq. (3) is obtained from Eq. (2) for a translation in one direction. Eq. (3) is obtained by transforming the added-mass equation of a circle of radius $r$ into a flat plate of length $2r$. For arbitrary foil sections, however, no analytical formula can be easily derived. In the case of numerical simulations, the velocity potential must be computed at each iteration, increasing computational cost.

### 2.2 *Added-Mass formulation for tidal turbine blades*

Maniaci & Li, 2012 estimate the added-mass on a tidal turbine blade, assuming that the blade section could be approximated as a flat plate of length $c$. The equation for a 2D blade section is expressed as:

$$m_{Blade} = \rho\pi\frac{c^2}{4} \tag{4}$$

where $c$ is the blade chord.

For a three-dimensional blade section, Eq. (4) is changed by multiplying the element length $dr$ :

$$m_{3D\,BE} = \rho\pi\frac{c^2}{4}dr \tag{5}$$

Eq. (5) has not been verified in the literature to the best of our knowledge.

### 2.3 *CFD Model*

Three sets of simulations are used in this study: a fixed foil at different angles of attack $\alpha$, an oscillating cylinder, and an oscillating foil. The RISØ-A1-24 is used in the airfoil cases. Characteristics are presented in Bertagnolio et al., 2001. The oscillating cylinder cases are simulated to verify the added-mass computation method presented in Section 2.4.

Simulations are conducted using RANS CFD with OpenFOAM v2212. The RANS model is used in several tidal rotor studies (e.g., Afgan et al., 2013; McNaughton et al., 2012), and has been tested and validated for dynamic stall problems (Rezaeiha et al., 2019). Turbulence is modelled with the $k-\omega\ SST$

closure with the updated coefficients of Menter et al., 2003, along with a wall-resolved boundary layer (maximum $y^+$ of 1.4). The turbulence intensity is set to $8\%$. This values is chosen to be similar to other studies on tidal turbines. The values for turbulence kinetic energy $k$, the specific turbulence dissipation $\omega$ and flow velocity $U_\infty$ are $k = 0.0864 \quad [m^2.s^{-2}]$, $\omega = 29.4 \quad [s^{-1}], U_\infty = 3 \quad [m.s^{-1}]$

The forces are computed during the simulation with an OpenFOAM function. Pressure and viscous forces are computed by integrating pressure and wall shear stresses on the blade surfaces.

At the maximum, the $y^+$ value equals $1.4$, which is in the optimal value range to compute boundary layer effects.

Two inflow speeds are considered. A fixed velocity inlet condition of $3\ m.s^{-1}$ and $6\ m.s^{-1}$ are imposed, with an inlet-outlet condition at the outlet of the domain.

The dynamic mesh module of OpenFOAM is used to simulate body oscillations. The oscillating condition models time-varying position, velocity and acceleration for the different amplitudes and frequencies studied, enabling the determination of added-mass effects.

A diagram of the numerical domain, including dimensions and boundary conditions, can be found in Fig. 1.

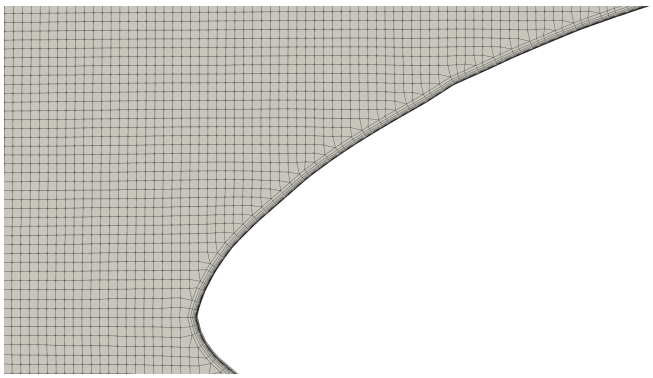

Figure 2: Boundary layer on the foil

### 2.4 *Added-mass computation*

The body motions affect the surrounding fluid which results in applied force on the structure. This force can be modelled through Morison's equation (Morison et al., 1950) :

$$F = \rho C_M V(\dot{u} - \dot{v}) + \frac{1}{2}\rho C_D A(u - v)\,|u - v|$$

$$= \rho V(\dot{u} - \dot{v}) + \rho C_A V(\dot{u} - \dot{v}) + \frac{1}{2}\rho C_D A(u - v)\,|u - v| \quad (6)$$

with $\rho$ the fluid density, $C_M$ = 1 + $C_A$ the inertia coefficient, $C_A$ the added-mass coefficient, $V$ the body volume, $u$ the oscillating flow velocity and $v$ the body velocity, $C_D$ the drag coefficient and $A$ the cross-sectional area. The first term represents the force proportional to the added-mass and the second term represents the drag component with $u$ the oscillating flow velocity. Here, the flow velocity is considered to be zero in the y-direction. In our cases of study, $\dot{u} = 0$ because of the prescribed steady inflow condition. Thus, the applied force on the foil profile is :

$$F = -\rho C_A V \dot{v} - \frac{1}{2}\rho A C_D v\,|v| \quad (7)$$

The foil motion is imposed in the transverse direction. At the first time-step, the geometric center is at $y(t = 0) = 0$. The prescribed motion is :

$$y(t) = A_m sin(\omega t) \;\Rightarrow\; v(t) = A_m \omega cos(\omega t) \quad (8)$$

with $A_m$ the amplitude and $\omega$ the frequency of motion.

The added-mass is found from the force with a least-square fit on Morison's equation (Eq. (7)). The model function is :

$$F_{model} = \rho C_A V A_m \omega^2 sin(\omega t) - \frac{1}{2}\rho A C_D A_m \omega cos(\omega t)\,|A_m \omega cos(\omega t)| \quad (9)$$

$\rho C_A V$ = $m_a$ and $\frac{1}{2}\rho A C_D$ are determined through the function fit, and only the added-mass term is investigated.

### 2.5 *Mesh Convergence Study*

The mesh is generated with OpenFOAM. It contains 4 refinement areas around the foil profile. The profile is snapped into the global mesh with SnappyHexMesh. A fine extruded mesh layer is added as seen in Fig 2.

A mesh convergence assessment is performed to determine the suitability of the domain discretisation. We used the Grid Convergence Index (GCI) developed Roache, 1997 to determine the mesh convergence from three different grid : coarse, medium and fine. The refinement ratio is constant between each grid and is defined as :

$$r = \sqrt{\frac{N_{fine}}{N_{medium}}} = \sqrt{\frac{N_{medium}}{N_{coarse}}} = 2 \quad (10)$$

with $N_i$ the number of cells for $i$ mesh. To characterize error, the lift coefficients at the angle of attack $\alpha = 0$ are used :

$$C_L = \frac{L}{\frac{1}{2}\rho A U_\infty^2} \quad (11)$$

Table 1: Mesh analysis with Grid Index Convergence

| Number of cells | Refinement factor | Lift coefficient $C_L$ | Error | GCI |
|---|---|---|---|---|
| [-] | [-] | [-] | [%] | [%] |
| 1.101 M | 4 | 0.4055 | - | - |
| 4.393 M | 2 | 0.38534 | 5.23 | 7.77519 |
| 17.547 M | 1 | 0.39629 | 2.92 | 4.10644 |

with $L$ the lift force, $\rho$ the fluid density, $A$ the foil surface area and $U_\infty$ the flow velocity. The lift coefficient for the fine, medium and coarse grids are respectively referred to as $f_1$, $f_2$ and $f_3$. The GCI between two grids is defined as :

$$GCI = \frac{F_S\,|e|}{r^p - 1} \tag{12}$$

with $|e|$ the relative error between meshes, $p$ the convergence order

$$p = \frac{ln(\left|\frac{f_3 - f_2}{f_2 - f_1}\right|)}{ln(r)} \tag{13}$$

$F_S$ is a safety factor. For three grids, the chosen value is $1.25$.

Grid convergence index results are presented in Table 1. The relative error and the GCI are low between meshes. The medium mesh is considered the best compromise between accuracy and computational costs for this study.

## 3 RESULTS AND DISCUSSION

### 3.1 *RISØ-A1-24 steady-state polar coefficients*

Lift and drag coefficients for the RISØ-A1-24 are compared to the results of the experimental campaign presented in Bertagnolio et al., 2001. The profile was tested in a wind tunnel at Reynolds number $Re = 1.6.10^6$ and Turbulent Intensity $T_u = 1\%$. Numerical simulations with the medium mesh and identical inflow conditions lead to the results presented in Fig. 3. The plots show lift ($C_L$) and drag ($C_D$) coefficients as a function of angle of attack $\alpha$.

The numerical results agree well with the experiments for both lift and drag. At low angles of attack, the drag coefficient from numerical simulation exceeds the experiment, while $C_L$ shows a much better agreement throughout the analysed range. $C_D$ is strongly affected by viscous forces and is typically more sensitive than $C_L$, which can explain the difference observed between the two sets of coefficients.

Above $\alpha$ = 12°, flow separation and vortex shedding phenomena start to occur. We observe that the

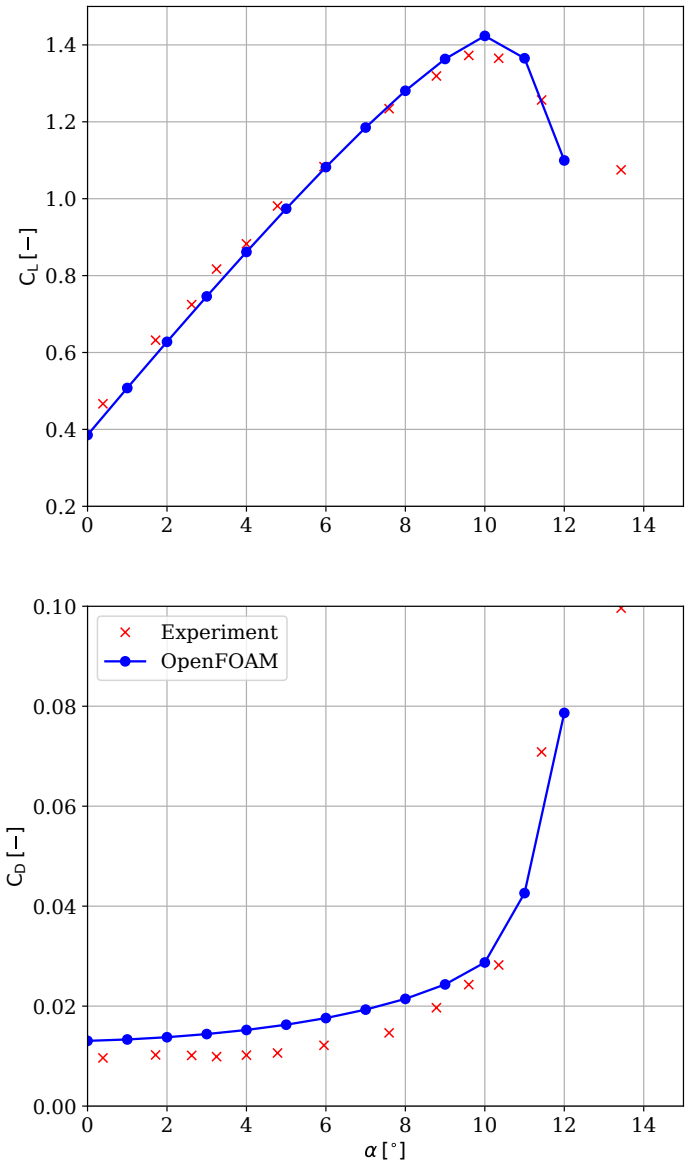


Figure 3: Lift coefficient (up) and drag coefficient (down) for the RISØ-A1-24 profile

CFD simulations successfully capture the onset of stall and the post-stall lift and drag with a good degree of agreement with the experiments.

### 3.2 *Added-mass*

The studied geometries are subjected to a forced motion in the transverse direction. The fluid mass displaced by the body during its acceleration is assumed

to be proportional to body acceleration to determine the volume of influence and the added-mass coefficients.

### 3.2.1 *Cylinder added-mass*

To test the function fit method, an oscillating cylinder is studied. This shape has been thoroughly investigated in literature (Blackburn & Henderson, 1999). OpenFOAM is not able to perform 2D simulation. Quasi-2D cases are represented as 3D geometries with one thin cell in the normal direction, which requires 3D added-mass equations. The theoretical 3D cylinder added-mass is defined as :

$$m_{a_{cylinder}} = \pi \rho r^2 H \tag{14}$$

with $r$ the cylinder radius and $H$ the height. In this study, $r$ is $0.5\ m$ (consistent with the $1\ m$ chord used for the airfoil) and $H$ is $0.002\ m$, which gives a theoretical added-mass of $1.5708\ kg$. Amplitude and frequency considered are :

$$\begin{cases} A_m &= 0.2\ m \\ \omega &= 5\ rad.s^{-1} \end{cases}$$

The least-square method is applied on peaks only, and not on the full signal. Limiting the input data to the peaks improves the precision of the function fit by avoiding the over-representation of mid values and focusing on the engineering-relevant maxima and minima. Forces applied during the oscillation and the fitted function from Eq. (9) with the obtained coefficients (blue) and the theoretical $C_A$ and $C_D$ (Brennen, 1982; Gao et al., 2018) are shown in Fig 4. The

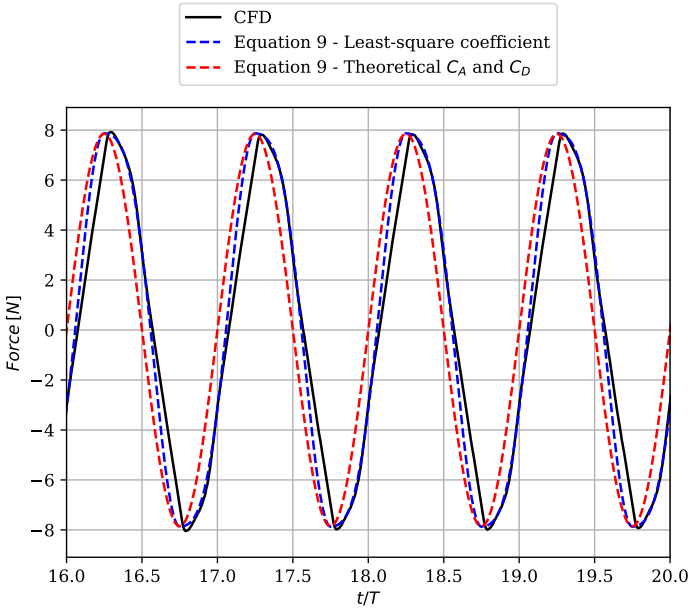


Figure 4: Measured force on the cylinder (black), the least-square fit with the coefficient on the Morison equation (blue) and with the theoretical added-mass and drag coefficient (red).

least-square function does not fit exactly the CFD-computed force in the transverse direction. This is explained, at least partially, by the vortex shedding occurring at maximum displacement. Fig 5 shows the phenomena during the upward and downward oscillation. The pressure field around the cylinder strongly decreases with the motion. Integrated pressure is rapidly modified, which leads to force modifications at maximum amplitude. The results suggest that the least-square fit could be improved by adding other harmonic terms in Eq. (9).

The returned added-mass coefficient $C_A$ in the case of the cylinder is $C_A = 1.0023$. Comparing the obtained value with the theoretical added-mass coefficient values of 1 (Maniaci & Li, 2012), the least-square method returns an accurate result. However, while the function fit captures the amplitudes well enough, a phase is observed between Morison's model and the CFD results. This difference is attributed to the vortex shedding discussed previously and other non-linearities not considered in the simplified model.

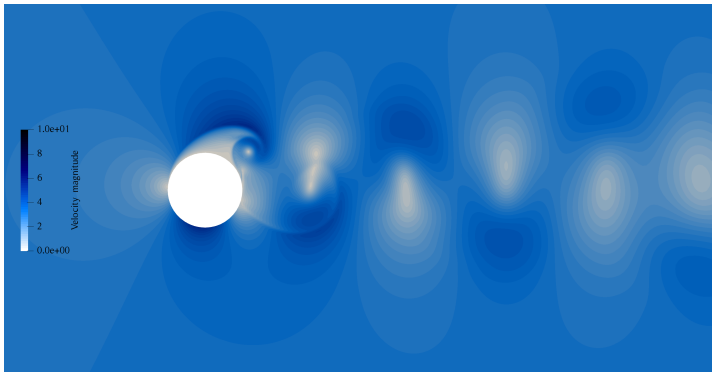


Figure 5: Velocity field around the cylinder during downward oscillation

### 3.2.2 *RISØ-A1-24 added-mass*

The amplitude and the frequency change the interaction between the structure and the flow. Three different amplitudes (0.2, 0.5, 0.8) $m$ and frequencies (2, 5, 10) $rad.s^{-1}$ are considered to study the added-mass effects on this airfoil.

Fig. 6 shows a motion amplitude of $0.2\ m$ and a frequency of $5\ rad.s^{-1}$, with an inflow speed of $3\ m/s$. Forces on the foil and the least-square fit with Eq. (9) are presented in the plot. Forces are lift-corrected by plotting the measured force with the mean force subtracted. Non-symmetric foil geometry causes additional effects. Similar vortex shedding, compared to the cylinder, is observed at maximum and minimum displacements are observed for the foil. During the downward oscillation, the measured force is higher. The lower foil part is concave, which results in a larger perturbation of fluid. The flow around the section is presented in Fig 7. Concerning the added-mass, the value is obtained from Eq. (5) with an element length set to $0.002\ m$ is $1.5708\ kg$.

For these parameters, the least-square function returns the following added-mass coefficient $C_A =$

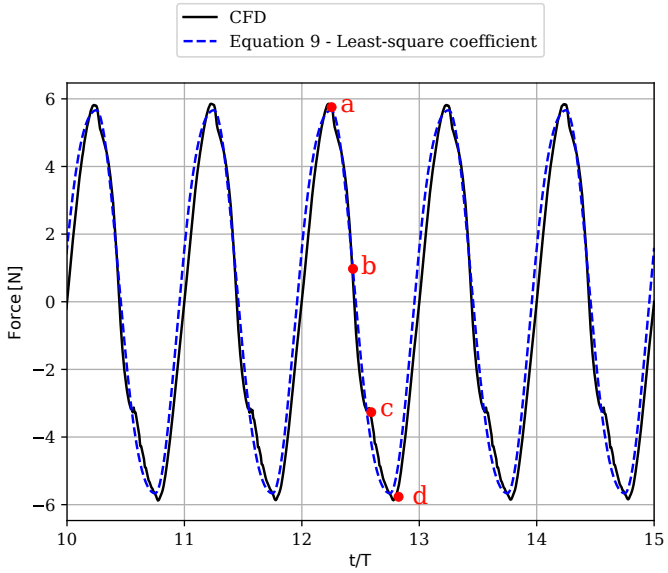


Figure 6: Measured forces applied on the foil profile. Corresponding velocity fields at points **a**, **b**, **c** and **d** are presented in Fig 7

0.7211. With this geometry and for this case, the relative error between the numerical simulation and the theoretical formulation increases to 28 % compared to the flat-plate assumption of Maniaci & Li, 2012. Errors start to become important for the foil profile.

Force variations are observed during the motion. On point $a$ on Fig 6, the force decreases rapidly after reaching the maximum. On point $c$, the applied force slightly increases during the downward oscillating. These variations represent other phenomena that are not considered in the Morison's Equation.

Fig. 8 shows a fast Fourier transform on the force obtained with the CFD. The prescribed motion frequency is 0.79 $Hz$, seen as the main peak in the plot, but other harmonics are also observed. Morison's model considers two components of identical frequency in quadrature (speed and acceleration). Considering these other harmonics in the aim function (Eq. (9)) could improve the fit with the least-square method, although without necessarily improving the physics of the underlying model. Extending the analysis to the rest of the simulated cases shows varying levels of discrepancy between CFD and the simplified model. Table 2 shows the different added-mass coefficient values for three $\omega$ (2, 5, 10) $rad.s^{-1}$, $A_m$ (0.2, 0.5, 0.8) $m$ and the two different inflow speeds (3, 6) $m.s^{-1}$.

A parametric dependency is observed for the added-mass coefficients on frequency, amplitude, and inflow speed. At constant amplitude, added-mass coefficients decrease as frequency increases. For a constant $\omega$, $C_A$ decreases as amplitude increases. At $\omega$ = 2 and $A_m$ = 0.2, the gap between CFD and the flat-plate assumption reaches 79.51 %, suggesting that the simplified model discussed in this work might not be suitable for practical applications.

Added-mass variations are similar for the 6 $m.s^{-1}$ inflow velocity cases, but with significant differences

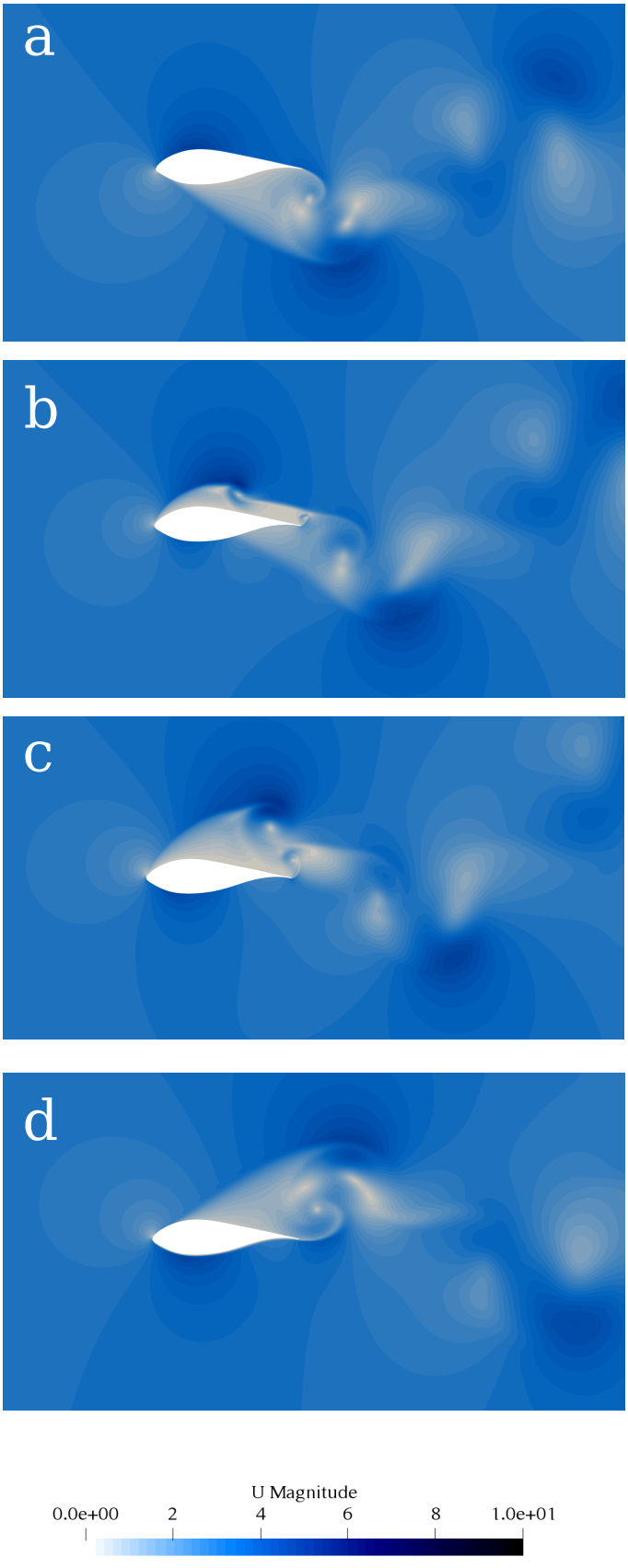


Figure 7: Velocity field around the blade section at three different times.

observed. For the minimum amplitude and frequency, the added-mass difference between two inflow speeds reaches 73.69 %. Besides sensitivity to amplitude and frequency, the inflow velocity is highlighted as the most important parameter affecting the added mass coefficients.

While an inflow speed of 6 $m.s^{-1}$ is unlikely in a

Table 2: Parametric study - Values on the table represent the added-mass coefficient at the given amplitude and frequency and two inflow velocity

| $A_m$ \ $\omega$ | 2 | 5 | 10 |
|---|---|---|---|
| 0.2 | 4.8805 | 0.7211 | 0.1232 |
| 0.5 | 2.7503 | 0.4147 | 0.1284 |
| 0.8 | 1.7655 | 0.3238 | 0.1245 |

a) $U_\infty = 3\,m.s^{-1}$

| $A_m$ \ $\omega$ | 2 | 5 | 10 |
|---|---|---|---|
| 0.2 | 19.107 | 3.1208 | 0.7377 |
| 0.5 | 9.3613 | 1.6475 | 0.4016 |
| 0.8 | 6.2453 | 1.1529 | 0.2957 |

b) $U_\infty = 6\,m.s^{-1}$

tidal channel (e.g., the mean velocity in the Raz Blanchard is around $2\,m.s^{-1}$ (Bailly du Bois et al., 2020)), the relative inflow speed on a rotating blade section can exceed the range of speeds analysed in this work.

## 4 CONCLUSION

The added-mass effects have been studied on two geometries: a cylinder and a RISØ-A1-24 profile. After a mesh convergence study with the Grid Convergence Index, RISØ-A1-24 polar coefficients were computed and compared with experimental measurements. Computed results were in good agreement with the experimental data for drag and lift coefficients.

Fitting the CFD data of the prescribed motion simulations to Morison's engineering model was first tested with an oscillating cylinder to compute added-mass coefficients. The cylinder coefficient derived from the CFD results is nearly identical to the theoretical value, and both models show a good agreement in peak amplitudes, although with a phase-difference. The difference is attributed to boundary layer separation occurring during the oscillation and other phenomena not considered by the engineering model.

The simulations of the RISØ-A1-24 airfoil under prescribed motions show that added-mass coefficients depend on parameters such as motion amplitude and frequency. The CFD results divert significantly from the simplified assumptions found in literature, and more importantly with errors that vary with the input parameters tested in this study.

Improving the predictions of Morison's equation could be done by parametrising the added mass coefficients, based on a large suite of simulations and tabulating results as functions of amplitude, frequency, in-

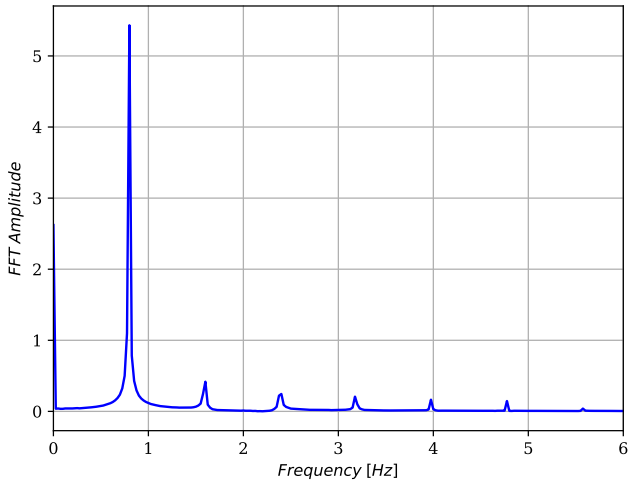


Figure 8: Fourier analysis of the applied force in the transverse direction for $\omega = 5\ rad.s^{-1}$ and $A_m = 0.2\ m$

flow speed, and foil geometry. The generality of such an approach, however, would remain arguable. This suggests that an improved model might be required to accurately capture added-mass effects on foils and tidal rotor blades.

While extra harmonics could also be considered in the function fit, it is likely that changes in the fundamentals of the engineering model model might yield a better reproduction of what is otherwise a very complex fluid phenomenon.

## ACKNOWLEDGEMENTS

The present work was performed on computing resources provided by CRIANN (Normandy, France). This project also received funding from the European Union's Horizon 2020 research and innovation programme under the Marie Skłodowska-Curie grant agreement No 101034329, and recipient of the WINNINGNormandy Program supported by the Normandy Region. The authors acknowledge the financial support from Normandy Region through the Laboratoire d'Excellence Energy, Materials and Clean Combustion Center (LabEx EMC3) and the Graduate School Materials and Energy Sciences (GS-MES).

## REFERENCES

Afgan, I et al. (2013). "Turbulent flow and loading on a tidal stream turbine by LES and RANS". In: *International Journal of Heat and Fluid Flow* 43, pp. 96–108.

Bailly du Bois, Pascal et al. (2020). "The Alderney Race: general hydrodynamic and particular features". In: *Philosophical Transactions of the Royal Society A* 378.2178, p. 20190492.

Bertagnolio, Franck et al. (2001). "Wind turbine airfoil catalogue". In.

Blackburn, Hugh M & Ron D Henderson (1999). "A study of two-dimensional flow past an oscillating cylinder". In: *Journal of Fluid Mechanics* 385, pp. 255–286.

Brennen, Christopher Earls (1982). "A review of added mass and fluid inertial forces". In: *Naval Civil Engineering Laboratory*.

Faudot, Céline & Ole Gunnar Dahlhaug (2012). "Prediction of wave loads on tidal turbine blades". In: *Energy Procedia* 20, pp. 116–133.

Gao, Wenjun et al. (2018). "Numerical investigations on drag coefficient of circular cylinder with two free ends in roller bearings". In: *Tribology International* 123, pp. 43–49.

Ghassemi, Hassan & Ehsan Yari (2011). "The added mass coefficient computation of sphere, ellipsoid and marine propellers using boundary element method". In: *Polish Maritime Research* 18.1, pp. 17–26.

Guo, Xiaoxian et al. (2018). "The surface wave effects on the performance and the loading of a tidal turbine". In: *Ocean Engineering* 156, pp. 120–134.

Javanmard, Ehsan, Shahriar Mansoorzadeh & Javad A Mehr (2020). "A new CFD method for determination of translational added mass coefficients of an underwater vehicle". In: *Ocean Engineering* 215, p. 107857.

Lefrançois, Emmanuel (2017). "How an added mass matrix estimation may dramatically improve FSI calculations for moving foils". In: *Applied Mathematical Modelling* 51, pp. 655–668.

Lou, Benqiang & Hongyu Cui (2021). "Fluid–structure interaction vibration experiments and numerical verification of a real marine propeller". In: *Polish Maritime Research* 28.3, pp. 61–75.

Maniaci, David C & Ye Li (2012). "Investigating the influence of the added mass effect to marine hydrokinetic horizontal-axis turbines using a General Dynamic Wake wind turbine code". In: *Marine Technology Society Journal* 46.4, pp. 71–78.

McNaughton, James et al. (2012). "CFD prediction of turbulent flow on an experimental tidal stream turbine using RANS modelling". In: *1st Asian Wave and Tidal Energy Conference*.

Menter, Florian R, Martin Kuntz & Robin Langtry (2003). "Ten years of industrial experience with the SST turbulence model". In: *Turbulence, heat and mass transfer* 4.1, pp. 625–632.

Moelyadi, Mochammad Agoes & Bagus Bambang Riswandi (2018). "CFD based added mass prediction in cruise condition of underwater vehicle dynamic". In: *Journal of Physics: Conference Series*. Vol. 1005. 1. IOP Publishing, p. 012011.

Morison, J R, Joseph W Johnson & Samuel A Schaaf (1950). "The force exerted by surface waves on piles". In: *Journal of Petroleum Technology* 2.05, pp. 149–154.

Murray, Robynne E, Robert Thresher & Jason Jonkman (2018). "Added-mass effects on a horizontal-axis tidal turbine using FAST v8". In: *Renewable Energy* 126, pp. 987–1002.

Parsons, Michael G, William S Vorus & Edward M Richard (1980). *Added mass and damping of vibrating propellers*. Tech. rep. University of Michigan.

Rezaeiha, Abdolrahim, Hamid Montazeri & Bert Blocken (2019). "CFD analysis of dynamic stall on vertical axis wind turbines using Scale-Adaptive Simulation (SAS): Comparison against URANS and hybrid RANS/LES". In: *Energy Conversion and Management* 196, pp. 1282–1298.

Roache, Patrick J (1997). "Quantification of uncertainty in computational fluid dynamics". In: *Annual review of fluid Mechanics* 29.1, pp. 123–160.

Satrio, D et al. (2024). "The Advantages and Challenges of Carbon Fiber Reinforced Polymers for Tidal Current Turbine Systems-An Overview". In: *IOP Conference Series: Earth and Environmental Science*. Vol. 1298. 1. IOP Publishing, p. 012029.

Schluntz, Justine & Richard HJ Willden (2015). "The effect of blockage on tidal turbine rotor design and performance". In: *Renewable Energy* 81, pp. 432–441.

Sedlar, Damir, Z Lozina & D Vucina (2011). "Experimental investigation of the added mass of the cantilever beam partially submerged in water". In: *Technical Gazette* 18.4, pp. 589–594.

Zhang, Liang et al. (2015). "The effects of surge motion of the floating platform on hydrodynamics performance of horizontal-axis tidal current turbine". In: *Renewable energy* 74, pp. 796–802.

Zilic de Arcos, Federico, Christopher R Vogel & Richard HJ Willden (2023). "A numerical study on the hydrodynamics of a floating tidal rotor under the combined effects of currents and waves". In: *Ocean Engineering* 286, p. 115612.

Zilic de Arcos, Federico, Christopher R Vogel & Richard HJ Willden (2022). "A parametric study on the hydrodynamics of tidal turbine blade deformation". In: *Journal of Fluids and Structures* 113, p. 103626.